Engineering Failure Analysis 43 (2014) 253–270

Contents lists available at ScienceDirect

Engineering Failure Analysis

journal homepage: www.elsevier.com/locate/engfailanal

Investigations on the breakdown of a heat recovery steam generator during the initial operation run

D. Bettge *, C. Klinger, D. Klingbeil, A. Eberle

Federal Institute of Materials Research and Testing (BAM), Berlin, Germany

ARTICLE INFO

Article history:
Available online 11 January 2014

Keywords:
Steam generator
Fatigue failure
Vibration analysis
Vibrations due to shipping

ABSTRACT

Several years ago, in 2003, an industrial heat recovery steam generator in charge of generating process steam in a petrochemical refinery was installed and prepared for initial operation. The steam generator enclosed an evaporator section and a superheater section consisting mainly of bundles of tubes with the longest up to several metres in length. During initial operation test runs severe leakages in the evaporator and superheater modules became noticeable. The test runs were stopped and after disassembly, through-wall cracks in several tube bends were found. BAM was commissioned to carry out the investigations in order to find out the reasons for the failure of the tubes. During on-site inspection a number of relevant damaged components and parts were selected and taken away to the laboratories for detailed inspection. Planned analyses were to comprise metallographic as well as fractographic investigations, mechanical fatigue testing and experimental as well as finite element vibration analyses on specimens and components. Soon, the fracture mechanism was found to be mechanical fatigue due to the fact that the examined fracture surfaces showed the very characteristic beachmarks and colouring patterns. To identify the particular loading and time at which crack initiation and crack propagation took place, experimental and numerical vibration analyses of specific tubes as well as mechanical fatigue tests on tube bends were carried out. Thus it was possible to identify the eigenfrequencies of individual tubes, to estimate the dynamic response as well as the nominal stresses and, hence, experimentally characterise the in-service fatigue strength of the components. Mechanical and thermal comparative tests on tube bends were performed simulating the conditions during the initial test run in order to get crack surfaces comparable to that of the originally damaged components. Thereby it became obvious that the fatigue cracks were initiated by vibrations the tube bundles were exposed to during rail transport from the manufacturer's site to the place of installation. Based on these results, the damaged components could be repaired or exchanged without modification of the construction, but the rules relating packaging and securing for shipping had to be revised.

1. Introduction

The recovery heat steam generator which is shown in Fig. 1 was installed in the exhaust air stream of a petrochemical refinery in 2003 in order to produce process steam. The steam generator embodied an evaporator unit with 6 evaporator modules as shown in Fig. 2 and sketched in Fig. 3.

* Corresponding author. Tel.: +49 3081041512; fax: +49 3081041517.
E-mail address: dirk.bettge@bam.de (D. Bettge).

http://dx.doi.org/10.1016/j.engfailanal.2013.12.005
1350-6307/

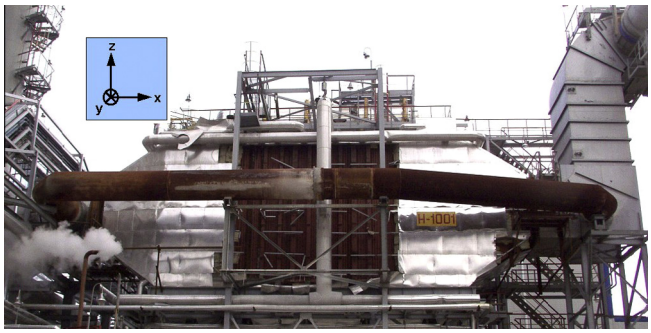

Fig. 1. Installation situation of the steam generator at a chemical plant, side view with temporary bypass tube. Coordinate "*x*" indicates the direction of airflow.

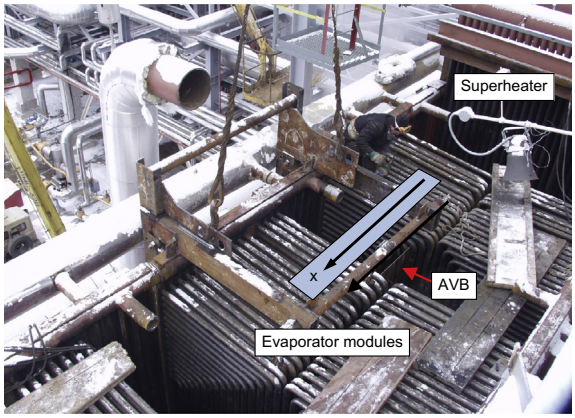

Fig. 2. Dismantling of the heat exchanger at the chemical plant. Top view of the evaporator. Arrow points to an anti-vibration plate (AVB). Coordinate "*x*" indicates the direction of airflow.

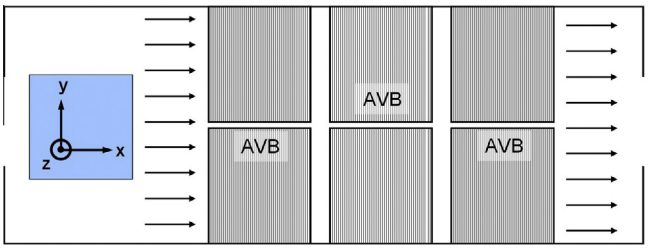

Fig. 3. Sketch of the positions of the six evaporator modules in the heat exchanger box, top view, compare Fig. 2. Arrows mark the exhaust air stream. "AVB" marks the positions of anti-vibration plates.

Each evaporator module was built from 15 pipe bends of different length nested as stacks and always 17 of this stacks were welded onto a finned wall, see Fig. 4. For shipping each evaporator module was fixed within a transport cradle. The distance for transport from the manufacturing site to the place of operation was about 2000 km. The largest section (1600 km) was realized by rail transport on a cargo waggon, as may be seen in Fig. 5. Only a small distance was covered on the road using a truck trailer. The heat exchanger was assembled at the site of operation and then tested extensively. In the course of these initial operation test procedures leakages were detected in the evaporator modules.

1.1. History of operation, failure and initial troubleshooting

The following facts concerning the history of operation, the detection of leakages and the initial troubleshooting were not performed by personnel of BAM, thus, are solely based on the descriptions given by the operator and the manufacturer.

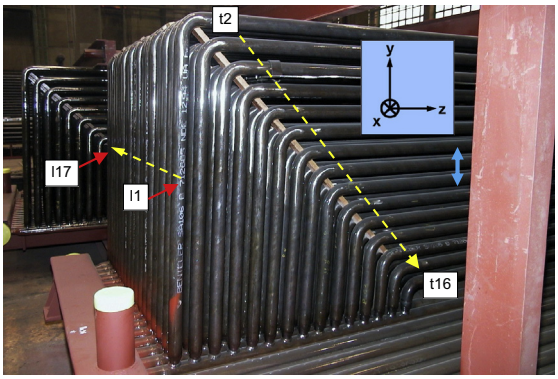

Fig. 4. Evaporator module fixed in a transport cradle. The tubes are numbered from "t2" (largest) to "t16" (smallest). Tube stacks are arranged from front to back in this image (numbered "l1" to "l17"); finned wall at the bottom, wooden laths left from manufacturing; vibration direction was in *y*-axis (blue arrow). (For interpretation of the references to colour in this figure legend, the reader is referred to the web version of this article.)

Fig. 5. An evaporator module fixed in a transport cradle and loaded onto a two-axles railroad cargo waggon for shipping. *Source:* customer

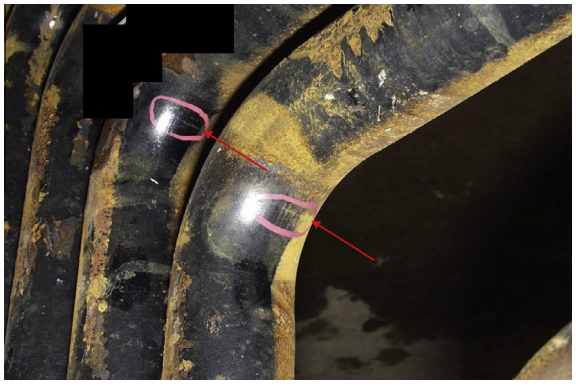

Fig. 6. Cracks (see arrows) found at the surface around the apex of the pipe bend in an evaporator module during on-site inspection.

The evaporator modules were built up of bended and welded pipes. After assembly each module was pressure tested successfully by the manufacturer at the production facility. For shipping the modules were packed into a transport cradle which was fixed on a railway cargo wagon, Fig. 5, as mentioned before. After shipping to the site of operation, the steam generator was assembled from 6 evaporator modules, the superheater and several other components.

As soon as the assembly of the steam generator at the site of operation was finished, the whole unit was tested for leak tightness by a hydraulic pressure test using twice the operating pressure. No indications for leakage were reported. After this, a test run involving the air blower was performed covering a range of 72 h at 50% of the rated power and at a temperature of 240 °C. After this run the following test for leak tightness revealed leakages within the evaporator modules, Fig. 6,

and within the superheater section. All tubes that exhibited leakages that were detected at that time were removed and the holes blinded.

Thereupon a further test for leak tightness revealed even more leakages and after some more unsuccessful attempts to remove furthermore damaged tubes and test the remaining units successfully, it was decided, to set the whole heat exchanger into bypass mode. This meant that it was circumvented completely by a tube of large diameter, as seen in Fig. 1. Thereby, the required process steam had to be provided by an external power plant.

1.2. Assignment of experts

At this time the parties may have estimated the monetary losses due to breakdown, repair, reinstallation and additional steam cost to several million Euros. This, undoubtedly, set questions about warranty and responsibility on the plan. Thus, the manufacturer, the distributor and the operator individually ordered investigations concerning the quality of the material at different laboratories and institutions. Seven reports resulted in different and partly contradicting causes for the failure, putting the blame on each of the other parties, respectively. With even the fracture mechanism not being clear, a repair and subsequent re-installation of the modules seemed to be too risky especially without having unquestionable information on the main source of the breakdown.

After some negotiations, manufacturer, distributor and customer agreed to commission an extensive analysis concerning the detection of the main cause of failure to experts of BAM. The arbitration opinion given in the expert report was supposed to be binding for all parties with respect to further decisions.

2. On-site inspections at the operation site and at the manufacturer's plant

The inspection plan as specified by BAM specialists comprised: General on-site inspection of the unit and its components at the operation site as well as on-site inspections of the production process of the components and modules at the manufacturing facilities.

2.1. On-site inspection at the operating site

After formal assignment specialists inspected the steam generator as well as its modules and components directly at the petrochemical plant where it had been installed and designated for operation. The preliminary inspection of the leaking tubes of the evaporator modules showed that all leakages were caused by cracks visible to the naked eye. The through-wall cracks were without exception located at the inside of the pipe bends, as may be seen in Fig. 6. Thereupon, specific cracked sections were selected, cut off the tubes and taken away for in-depth investigations at the authors' laboratories.

2.2. Inspection of returned components at the production facilities

After on-site inspection at the operation site, all evaporator modules, the superheater section and some other components were shipped back to the manufacturer. There, the components were inspected in detail, and additional test pieces were selected and taken away for further examination. Altogether, 35 test pieces were analysed and tested at BAM laboratories.

A very essential circumstance may be related to the packaging of the evaporator modules. Fig. 4 shows a module fixed on a transport cradle. It may be noticed that between each of two of the stacks a lath has been shoved diagonally. According to the manufacturer this construction, originally used for production as a spacer, was also used for transport to stem vertical shaking or vibration of the pipes.

2.3. Inspection of the tube bending process

The fact that the through-wall cracks in the evaporator tubes only occurred on the inner side of the pipe bends implicated that the bending process was studied at the manufacturer's site. The tubes were produced from a ferritic–perlitic steel and cold-formed using a semiautomatic machine. With the bending radius rather small, the steel was exposed to a high degree of plastic deformation and additionally the tube surface was scratched. These scratches were partially removed by grinding. According to the relevant ASME codes Section 1, Ed. 01 the bending process was performed within usual parameters. No specific issues were found during this inspection.

2.4. Inspection of the production of the modules and vibration analysis

The manufacturing of the evaporator modules was inspected at another plant of the manufacturer. Here, the welding of the tubes to the finned walls was observed.

Some already completed evaporator modules were stored in an orientation similar to the final position in the broken steam generator. Several of the longer tubes were equipped with accelerometers in the mid-section. This made it possible to translate some results from vibration analyses to results obtained by tests performed later at BAM laboratories. Hence,

individual tubes were excited manually and the decaying signals of the vibration amplitudes were recorded. In that early state of the investigation it became obvious that the tubes were rarely damped so that the decay of each of the amplitudes was very slow. Traveling waves were observed wandering through the stacks from tube to tube. Back at the laboratory, at a later time, the eigenfrequencies and damping characteristics of each of the tubes were to be evaluated.

3. Materials testing on original test pieces

Detailed investigations with regard to the microstructure of the material and the crack surfaces of the original test pieces of the pipe bends were carried out. These investigations comprised metallographic analyses of the base material as well as fractographic analyses of the crack surfaces of all test pieces cut off the original tubes. According to the specification, the pipes were manufactured from SA 106 Gr. B acc. ASME (standard specification for seamless carbon steel pipe for high temperature service), Section 2, seamless tubes 60.3 mm × 5.6 mm. The bend radius was 76 mm. This was verified by several preliminary inspections.

3.1. Position-dependent scatter of the leakages

According to the manufacturer, all pipe bends of the evaporator tubes were inspected concerning structural integrity by means of pressure tests. After the incident the modules of the evaporator were shipped back to the manufacturer and after disassembly they were tested using the eddy current method. In total, 1530 tubes with 3060 pipe bends were inspected. Only about 2% of the pipe bends were found to show cracks deeper than 1 mm. It was not possible to detect through-wall cracks with this method.

The position-dependent scatter of all cracked tubes which showed leakage was statistically evaluated and the results are shown in the charts of Figs. 7 and 8. The data consider indications for cracks deeper than 0.5 mm. The indications were related to the mounting position of the particular tube within the module. It may be stated that longer tubes were stronger affected than shorter ones. Other criterions referring to the mounting position of the pipe within the unit such as "top/bottom", "left/right" and "front/back", were found not to be significant.

3.2. Preparation of the original samples for materials testing

As reported earlier, several cracked pipe bends of specific evaporator tubes were selected and taken away for fractographic evaluation during the on-site inspection. The cracks were mechanically opened using the hydraulic testing system of Fig. 9. In order to do this, the pipe bends were cut off the tubes, and the sections were partially saw cut for the sake of a smaller cross-sectional area to pull apart. After crack opening ever two ring-shaped specimens were cut from one half of the section. Always one of these rings holds the fracture surface. The other ring was used for preparing a metallographic cross section, Fig. 10.

3.3. Metallographic analyses of original test pieces

The microstructure of the material of the evaporator tubes was analysed in general and especially at the pipe bends. In this paper only the microstructure of the bended sections is discussed. The images shown in Fig. 11 focus on the inner radius of the elbow near the crack. As expected, a ferritic–perlitic microstructure was observed. Distinctive plastic deformation and

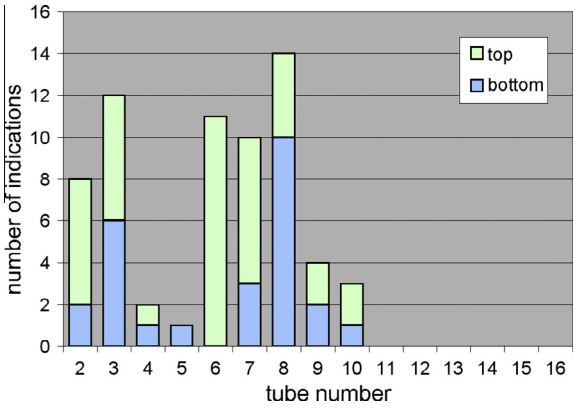

Fig. 7. Distribution of crack indications related to the tubes. Small tube numbers means large tube length. Tubes are numbered from "2" to "16" (see Fig. 4). Top elbows and bottom elbows are marked green and blue, respectively. Short tubes (11–16) did not fail.

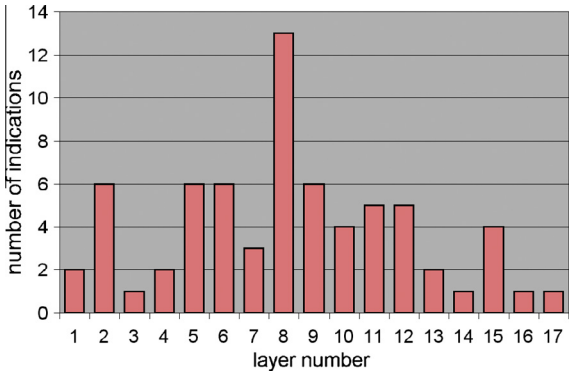

Fig. 8. Distribution of crack indications related to the tube layers (stacks) of the evaporator modules. Layers are numbered "1" to "17". Layer 9 is located in the centre of the module.

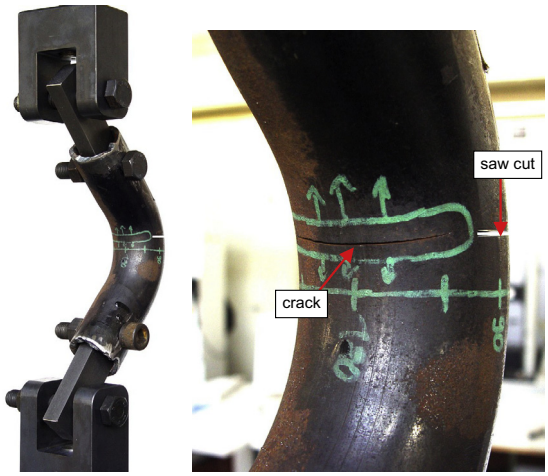

Fig. 9. Opening of a cracked pipe bend in the lab using a servo-hydraulic testing system.

Fig. 10. Part of the pipe bend after crack opening and cutting-off of 2 rings. The ring to the right comprises the crack surface of Fig. 12. The left ring was cut for metallographic investigations, see Fig. 11.

material overlap was found at the surface due to the bending process. It may be stated in advance that during the fractographic investigations it was seen that these surface features did not act as crack starters.

3.4. Macro- and micro-fractographic analyses of the crack surfaces

At first, the crack surfaces were investigated using the naked eye and a magnifying glass. Then the structures were analysed and documented using macrophotography, stereo microscopy and scanning electron microscopy (SEM).

After opening the cracks using the test machine shown in Fig. 9 the crack surfaces were prepared for fractography. Fig. 13 shows a photography of each of the two crack surfaces of an opened crack. The top view shows that the crack surfaces were

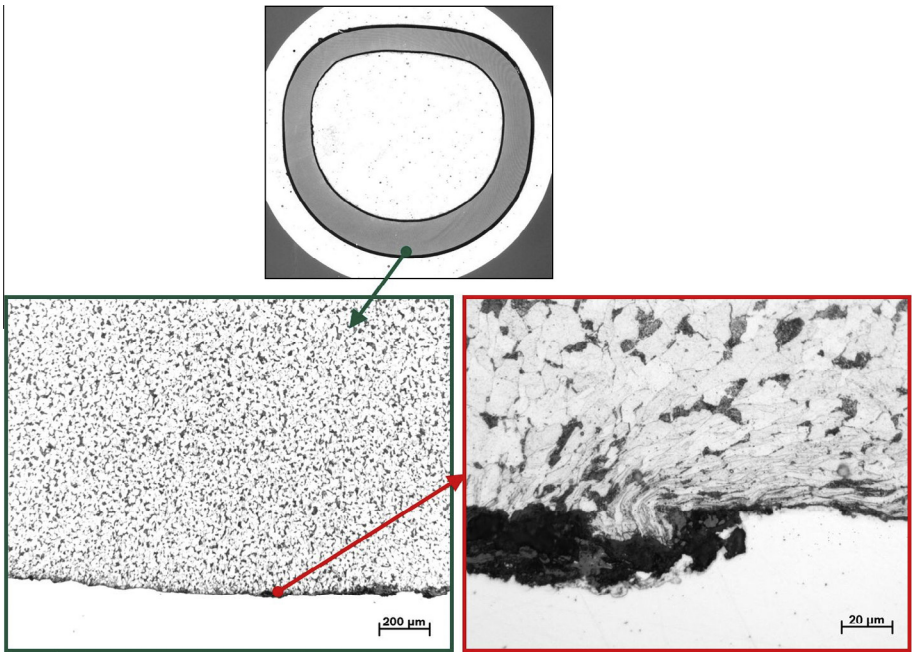

Fig. 11. Metallographic investigation of the microstructure of a cracked evaporator tube. For location of the cross section see Fig. 10. The cutouts focus on the inner radius near the crack. The microstructure is ferritic–perlitic. Plastic deformation at the surface is due to the bending process. The dots of the arrows give representative areas, not exact locations.

Fig. 12. Rings cut from the pipe bend of Fig. 10 containing the opened crack of Fig. 9. Lefthand: as opened; righthand: after removal of rust using citric acid.

clogged with coloured oxide layers, which were overlaid by rust. Nevertheless the circumferential character of the crack propagation may be noticed by a fine structure of rest lines. With the rust carefully removed using citric acid the graduation between the annealing colours was intensified and the rest lines between these colour schemes became clearly visible. A further series of cracks were opened and prepared for even the same detailed investigations and showed almost similar features, Fig. 14. From the documents of the operator regarding the pressure test runs it was not completely verifiable whether some of the pipes exhibited leakages already during testing. As a matter of fact, out of 7 cracks that were examined in the laboratory 5 were not yet cracked through the wall.

In order to illustrate the history of crack propagation by means of the crack surface of Fig. 13 in a better way, Fig. 15 was created. For this sake the crack starter point and several rest lines of semi-elliptical shape were plotted onto the crack surface in yellow colour. It may be seen that the crack not only propagates radially through the wall but even quicker circumferentially around the pipe wall. Adjacent to the circumferentially propagating crack and right in front of the surface from forced fracture by the laboratory a grey coloured crack area may be noticed ending with rest lines plotted in blue.

Taking the crack surface due to forced fracture by the laboratory unconsidered, the crack surface causing failure might now be divided into two zones of crack propagation. The first zone extends from the start of the crack along multiple yellow plotted rest lines to its final crack front plotted in blue. The crack surface is characterised by distinctive annealing colours and is denoted as fatigue crack growth region 1 in Fig. 15. In most cases the annealing colours on this first propagation area showed no correlation with the rest lines and, thus, might not be correlated with the crack propagation. This could be an indication that the annealing colours have been applied after this first period of crack propagation came to an end.

The second zone is characterised by a relative short crack propagation compared to the aforementioned zone of fatigue crack growth region 1 and propagates only along one blue rest line to the final crack front plotted in red. The related crack surface shows only weakly developed annealing colours. This zone is denoted as fatigue crack growth region 2 in Fig. 15.

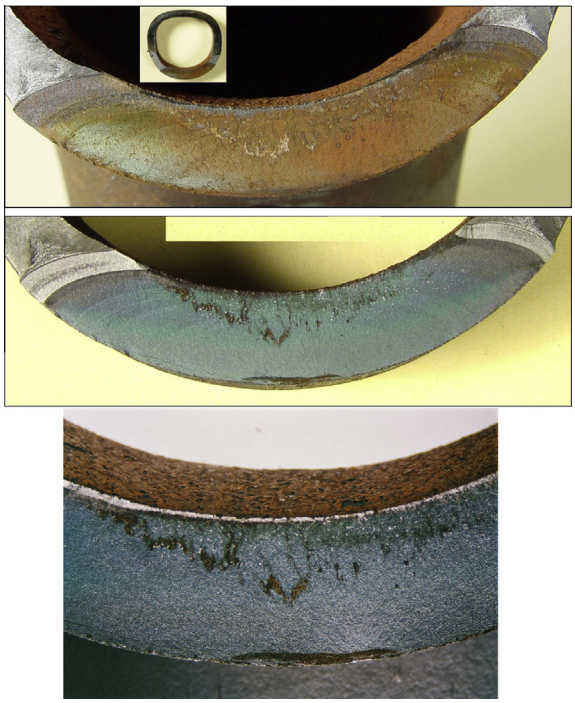

Fig. 13. Fracture surface found after opening a cracked tube. Enlargement of Fig. 12. Top: as opened; middle: after removal of rust using citric acid. Rest lines and annealing colours were found on the fracture surfaces, bottom: middle section, showing that coloured crack growth region has not grown through. (For interpretation of the references to colour in this figure legend, the reader is referred to the web version of this article.)

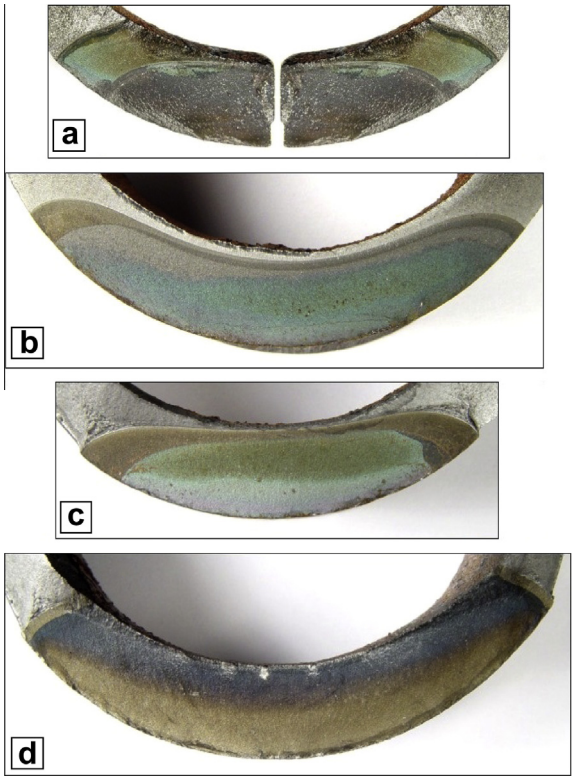

Fig. 14. Several additionally opened fatigue cracks imaged after rust removal by citric acid. The image of crack (a) was reconstructed from the previously separated crack surface.

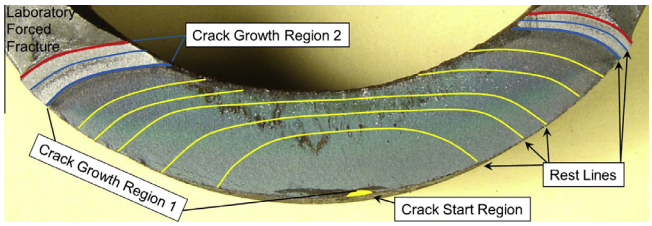

Fig. 15. Macroscopic characteristics of an opened crack surface. Crack starter and semi-elliptical rest lines (yellow) of fatigue crack growth region 1. Subsequent propagation of fatigue crack growth region 2 (blue rest lines) until final crack front (red lines). Forced fracture by crack opening in the lab (adjacent to the final crack front).

In a nutshell, the investigations on the macrostructure of all crack surfaces showed the same characteristics which may be summarized as follows:

- All cracks were fatigue cracks [1,2].
- The crack starter region always was located at the outer surface of the wall at the inner radius of the pipe bend, Fig. 15.
- The crack front was of a semi-elliptical shape as usual for fatigue cracks in circular tubes under bending loads [3].
- The crack surfaces were nearly planar.
- The crack plane was located some millimetres away from the apex of the elbow at the inner contour (intrados = ID). As long as the 45° apex plane is a plane of symmetry with respect to the geometry, loading and boundary conditions, the maximum normal stress will occur at this position. As soon as geometry as well as loads deviate from that symmetric condition, the stress maximum and, hence, the crack will no longer occur at the apex but at a small distance away from it. In Fig. 9 the apex of the elbow is indicated by the circumferential line.

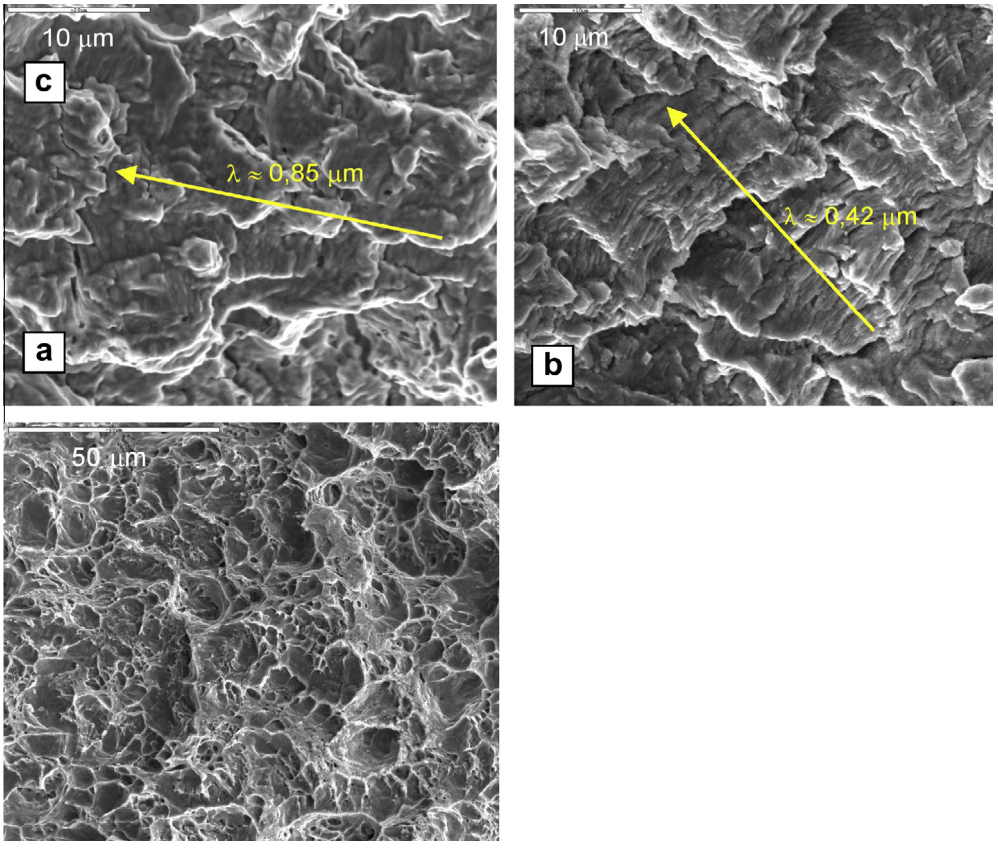

Fig. 16. SEM investigations of the fatigue crack. (a) Fatigue crack growth region 1 in Fig. 15: fatigue striations at the area near the end of the primary crack phase; (b) fatigue crack growth region 2 in Fig. 15: fatigue striations developed during the second phase of fatigue crack propagation; (c) laboratory forced fracture surface showing dimples.

- Rest lines (beachmarks) of semi-elliptical shape were observable on the crack surfaces (plotted in yellow and blue, in Fig. 15).
- The fatigue crack surface had two zones with different annealing colours and a different number of crack arrest lines. The colouring of these regions was not clearly defined for all investigated cracks. In most cases, however, the first region was the larger one and its annealing colours were more distinctive.
- Some cracks did not yet cause leakage, though, the circumferential crack propagation was already considerable, e.g. for cracks (b) and (c) in Fig. 14. This meant that the radial crack propagation was retarded. In case of semi-elliptical cracks this is a known phenomenon because crack propagation is mainly forced towards the very part of the ligament exhibiting the highest amount of triaxiality (this is the ratio between the hydrostatic and the equivalent stress). Regarding the present 3 dimensional stress state, the highest triaxiality should arise where the crack front is closer to the outer surface of the tube wall [4].

The SEM was used to analyse the microstructure of the crack surfaces. In Fig. 16 details of the analysed crack surface from Fig. 15 are shown. The former assumption of dealing with fatigue cracks was confirmed. Fatigue striations were identified in both zones of the crack surface of Fig. 15. The arrows in images (a) and (b) of Fig. 16 indicate the particular direction of crack propagation. By counting the number of striations for a certain length of crack propagation, an average width λ could be calculated for fatigue crack growth regions 1 and 2, respectively. Although this may be seen as estimation, it may be stated without doubt that the velocity of crack propagation of fatigue crack growth region 1 was generally higher than that of fatigue crack growth region 2.

Beyond the fatigue crack areas of the crack surface a honeycomb structure was found indicating ductile forced fracture due to crack opening. Furthermore this indicates that the material was able to undergo ductile deformation.

It seemed to be the case that at least in some instances the leakages developed very lately during crack propagation. Referring to cracks (a–c) in Fig. 14 the first phase of crack propagation did not lead to leakage. This implied the hypothesis that in some of the investigated tubes a first loading sequence caused a large amount of crack propagation, whereas later, a second loading sequence caused leakage.

4. Discussion of possible causes of failure

Following the results of the investigations and examinations as described in the preceding sections, it by now may be stated that failure mechanisms which were supposed not to generate fatigue crack failure may be excluded as root causes. This belongs mostly to mechanisms dedicated to all kind of static loading, namely:

- The manufacturing process including bending and welding of the tubes, as well as the module pressure tests.
- Handling before and after shipping.
- On-site installation.
- Static pressure tests of the evaporator on-site.
- Freezing of water within the tubes.

On-site installation and pressure tests may be seen to act as a secondary loading sequence. After eliminating the above mechanisms, only two failure mechanisms were left to play a role as root causes:

- The rail transport which produces extensive mechanical excitation for vibration.
- The test runs of the steam generator which leads to excitation due to the phenomenon of the von Karman vortex shedding. Thereby, a pattern of swirling vortices caused by a steady separation of flow of a fluid around blunt bodies will be formed depending on the Reynolds numbers.

Several reasons stood against the test runs as a source of failure. The most important reasons were:

- The misalignment of the annealing colours with regard to the specific crack propagation zones on the fracture surfaces. From Fig. 15 it may be seen that the rest lines of crack growth region 1 are not aligned to the boundaries of the annealing colours. Thus, it is evident that the annealing colours must have been generated after the crack had propagated.
- The two distinct zones of fatigue crack propagation (fatigue crack growth regions 1 and 2).

Therefore, damage due to tube vibrations during rail transport appeared to be the most probable main reason for the breakdown of the whole unit. In order to verify this hypothesis the following investigations were assigned:

- Estimation of vibrational excitation and response levels caused by rail transport.
- Measurements on the decay of vibrations in order to estimate the vibration response characteristics of the evaporator pipes.
- Numerical analysis and finite element simulation of the loading situation the pipe bends were exposed to.

- Mechanical comparison fatigue tests using original pipe sections.
- Thermal treatment of crack surfaces in order to create annealing colours comparable to the original ones.
- Fractography of fatigue tested alternate components and comparison to original crack surfaces.

5. Analysis of in-service loads and strength of components

5.1. Estimation of vibrations induced by rail transport

The transport of the evaporator modules was accomplished using two-axle railroad freight cars shown in Fig. 5. During running on the railway tracks the load floor of the wagons vibrated in a characteristic manner. The vibration spectrum depends on both the quality of the track superstructure and the vibration behaviour of the loaded wagon itself. Such frequency spectra of load floors of railway freight cars may be specified as random vibration. They are described in literature and in specific standards [5,6], see Fig. 17.

For the use as excitation for in-service strength tests a time history signal may be generated from such a vibration spectrum using a Gaussian distribution. As in reality the vibration time history signal is composed of load cycles of different amplitudes and frequencies, Fig. 18.

5.2. Evaluation of vibration behaviour by vibration measurements

The disassembled evaporator modules were used to carry out vibration testing, compare Section 2.4. The goal was to achieve realistic system parameters for numerical simulation of the tube vibrations. Experiments were conducted on the measurement of the vibration characteristics such as vibration response and damping behaviour of the tubes. Individual tubes were excited at their centre until vibrating in the primary eigenmode.

Characterising the vibration response of the different tubes, decay curves were recorded and evaluated for the individual eigenfrequencies and damping. The eigenfrequencies of the longer tubes were about 10 Hz, those of the medium length were around 14 Hz. Note that all of those eigenfrequencies are well within the excitation frequency range shown in Fig. 17.

The damping (expressed as log. decrement Λ [10]) was as low as 0.003. . .0.005, which is close to material damping [11]. Measurements with the wooden laths between the tube stacks showed that damping was now almost 10 times higher.

It was estimated that during the rail transport along a distance of ca. 1600 km at an average speed of about 50 km/h with an eigenfrequency of the specific tube of 14 Hz the number of load cycles accumulated to more than 1.6 million vibrations of different amplitudes.

5.3. Finite element analysis of the vibration response

Finite element analysis (FEA) [12] was applied to a complete double-elbow bent tube, connected to a finned wall. The simulation was carried out using fully transient calculation and implicit integration over time similar to [13]. In the simulation, the bent tube was vibrating nearly without damping. Rayleigh damping was introduced and increased until the calculated decay curves showed damping like those measured by the experiments on the tubes of the evaporator modules, compare Sections 2.4 and 5.2. A resonance magnification of about 35 led to high vibration amplitudes even when using small excitation amplitudes as shown in Fig. 19.

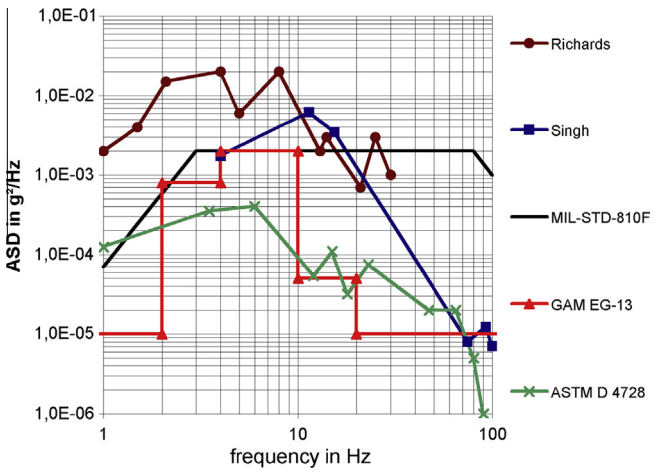

Fig. 17. Railway excitation spectra by different investigators [5,6] and standards [7–9]; random vibration expressed as acceleration spectral density (ASD) over the excitation frequency range of 1–100 Hz.

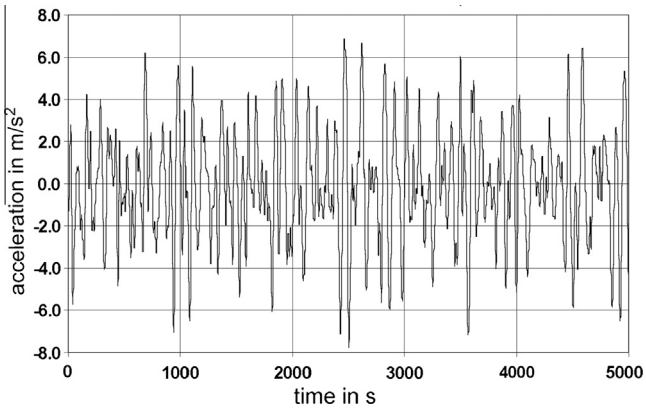

Fig. 18. Vibration time history used for excitation during simulation of rail transportation, generated from the envelope over the spectra in Fig. 17.

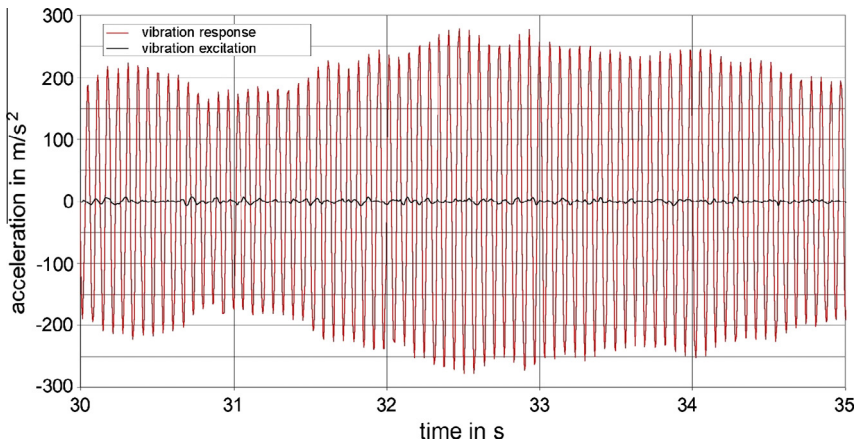

Fig. 19. Numerical simulation of the vibrations of an evaporator tube when transported by rail. Vibration response in the middle of the tube (red line) is much higher than vibration excitation at the foot (finned wall) on the rail transport waggon (black line). (For interpretation of the references to colour in this figure legend, the reader is referred to the web version of this article.)

5.4. Simulation of stresses and deformations

Using FEA the kind of stresses that would arise in the tube bend during vibration was simulated. Different vibration modes and their resonance frequencies were examined. The highest stresses emerged when vibrating in the first eigenform, as shown in Fig. 20. It was taken into account that the tubes were able to move at most 30 mm up and down. This deflection is half of the gap between each of the horizontal tubes of each two loops. The loops in a bundle are of different sizes in order to assemble them as a stack from small to large. Thus, it was postulated that each of the horizontal tubes should vibrate within the vertical plane of the stack with its own eigenfrequency and not in unison with other tubes. If the vertical deflection was to exceed 30 mm it was supposed that the horizontal tubes of each two loops would pound at each other. The highest computed tension and compression stresses were identical and around ±170 MPa. These stresses were located on the surface of the tube walls at the inner bend of the elbows (intrados = ID). The exact location was not at the apex of the tube bend, but some millimetres away. In our numerical simulation, the absolute values of the stresses on the ID and OD (extrados = OD) are identical because we used pipe elements with circular cross-section. This means that from the numerical simulation alone it cannot be decided whether a crack occurs on the ID or OD. After bending, the cross-section of the pipe is irregularly ovalised and no longer circular, Fig. 11. Typically, the distance from the centre of the cross-sectional area to the ID is longer than to the OD. This causes slightly larger stresses on the ID and results in cracks on the ID. Additionally, due to a fully plastic state of stress during manufacturing and spring-back after load release, tensile stresses will remain on the ID and compressive stresses on the OD. In case of the ID, the stresses from the manufacturing and loading have to be added whereas on the OD they have to be subtracted. Overall, these arguments imply higher tensile stresses on the ID than on the OD. As soon as the geometry (cross-section) as well as loads (deflection) of the structure deviate from a symmetric alignment the stress maximum will no longer occur at the apex of the pipe bend but at a small distance away from

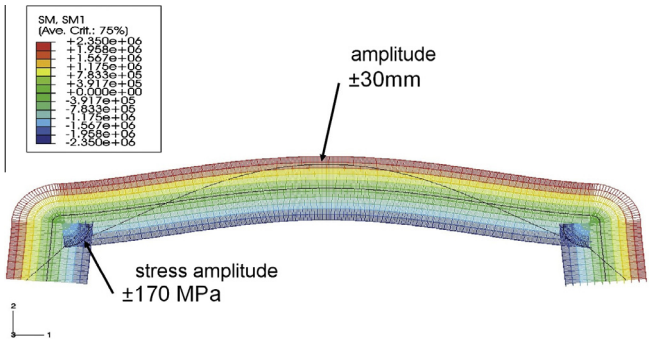

Fig. 20. Simulation of the stress distribution of an evaporator tube being deflected by an amplitude of 30 mm in the middle. Maximum tension stresses occurs at the tube bends. The legend shows values of the section moment.

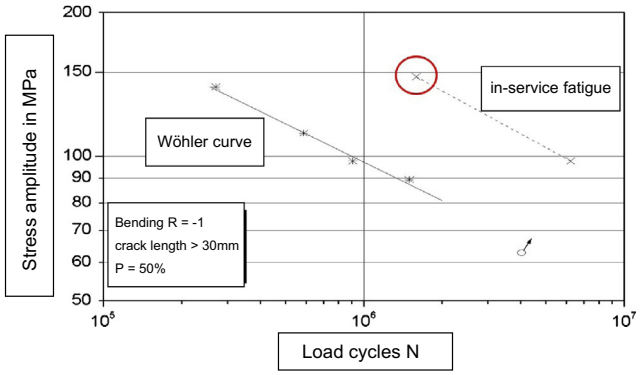

Fig. 21. Results of the fatigue tests using original tube bends.

it. This finding coincided with the location of the cracks documented during fractographic evaluation of the original failed tube bends, Fig. 6.

5.5. Comparative mechanical fatigue tests

By means of comparative component testing it was checked, whether the elbows could without damage withstand stresses of ±170 MPa as previously computed by FEA. Additionally, the fatigue cracks should be of a similar shape compared to those in the damaged parts. Therefore, elbows with pipe legs of about 50 cm in length were cut off undamaged tube elbows and prepared for testing.

In the beginning 5 Wöhler experiments with pure sinusoidal stress time history loads were carried out. The results were used to characterise the finite fatigue life strength of the elbow sections, Fig. 21. Furthermore two in-service fatigue tests under Gaussian load spectra, Figs. 21 and 22, were performed. These results were used to characterise the in-service fatigue strength of the tube elbows. The crack size found in the damaged parts was used as the failure criterion for fatigue testing.

When testing with about 100 MPa constant stress amplitude in the Wöhler experiment, the bend cracked almost through the wall at ca. one million cycles, Fig. 21. When using 100 MPa as the maximum stress amplitude and – as in service – a Gaussian load spectrum containing small amplitudes, too, the bend withstood almost 7 million load cycles, Fig. 21.

The test bend of the in-service fatigue strength test marked red[1] in Fig. 21 survived 1.6 million load cycles at a maximum stress amplitude of almost 150 MPa. Compared to the load cycles that were estimated to accumulate damage during rail transportation, compare Section 5.2, initiation of fatigue cracks due to vibrations during rail transport now seemed to be probable.

5.6. Thermal comparison tests

In a final step it was to generate proper annealing colours on the crack surfaces of the test specimens. This colouring should be as similar as possible to the colours found on the opened original crack surfaces. Therefore elbow sections that

[1] For interpretation of colour in Fig. 21, the reader is referred to the web version of this article.

Fig. 22. Fatigue test of an elbow section. State after fatigue cracking and subsequent forced opening of the crack.

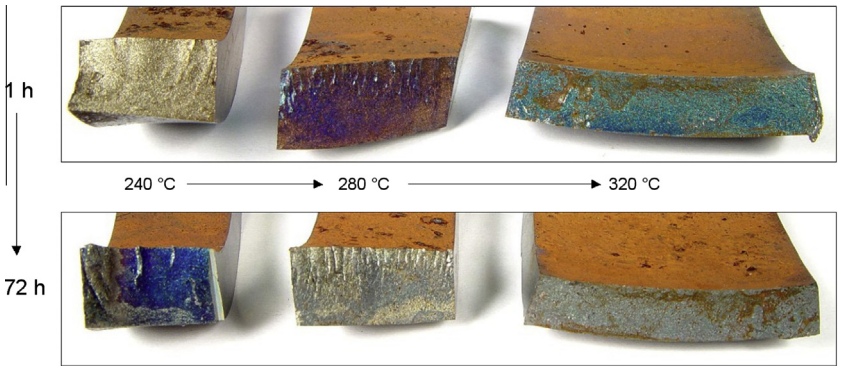

Fig. 23. Annealing colours on laboratory forced fractures after treatment in a furnace in air atmosphere; colour depending on time and temperature.

developed cracks during the mechanical tests were tempered within a chamber furnace before opening the cracks. Other samples came under further fatigue tests after tempering.

In order to find adequate limits for temperatures and annealing times, pre-tests were carried out on small laboratory forced fracture surfaces, Fig. 23. Data recording during the initial test run of the steam generator pointed to temperatures between 200 °C and 240 °C applied for drying the steam generator. To achieve annealing colours similar to that seen in Fig. 13, a heat treatment of 72 h at 240 °C was carried out, Fig. 24 top. Whenever the fatigue test was continued after the heat treatment, further effects such as formation of fretting were observed, Fig. 24 bottom.

On the annealed crack surfaces of the components tested as abovementioned, here and there some kind of porous coating was found using the SEM at normal magnifications, Fig. 27. At a much higher magnification, Fig. 28, some kind of whiskers was resolved on the crack surface. The whiskers were observed to be damaged by the electron beam of the SEM when imaged for more than some seconds. They were too small to be analysed using EDX. When re-investigating the original crack surfaces from the failure event with these pictures in mind, such a structure was found too, Figs. 25 and 26. Not all of the investigated fracture surfaces exhibited whiskers as may be clearly seen in these images. According to the literature the whiskers consist of iron oxide and grow on the surface when annealed in air, [14,15]. The whiskers found on the cracks of the elbow bends seem to grow under specific conditions in the slightly opened crack.

Fig. 24. Fracture surfaces of beforehand undamaged tube bends after laboratory mechanical fatigue test, followed by heating in a furnace and subsequent opening (upper specimen). Lower specimen was mechanically cycled after annealing and then opened.

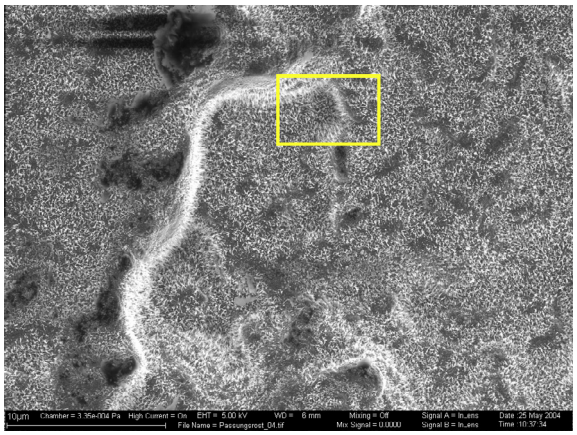

Fig. 25. Part of the fatigue fracture surface of an original fatigue crack, see crack surface (c) in Fig. 14. The crack surface is coated with small iron oxide whiskers.

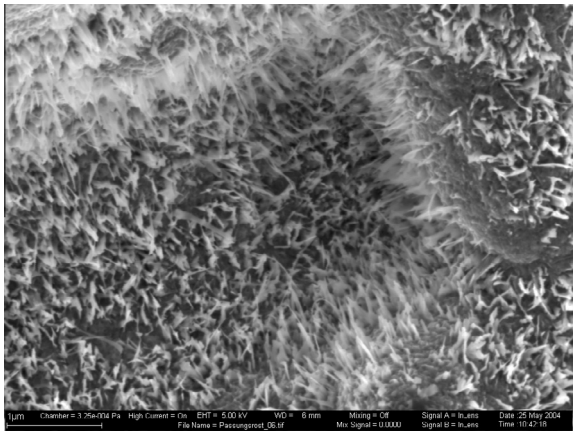

Fig. 26. Enlargement from Fig. 25. Iron oxide whiskers on the crack surface after annealing.

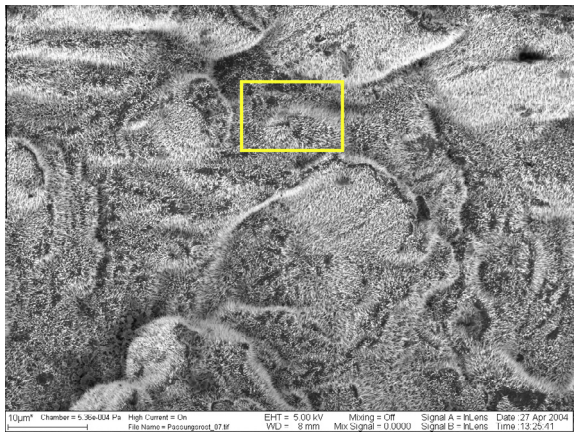

Fig. 27. Part of the fatigue fracture surface of a comparative component test after annealing. The crack surface is coated with small iron oxide whiskers grown during heat treatment in a furnace with ambient atmosphere.

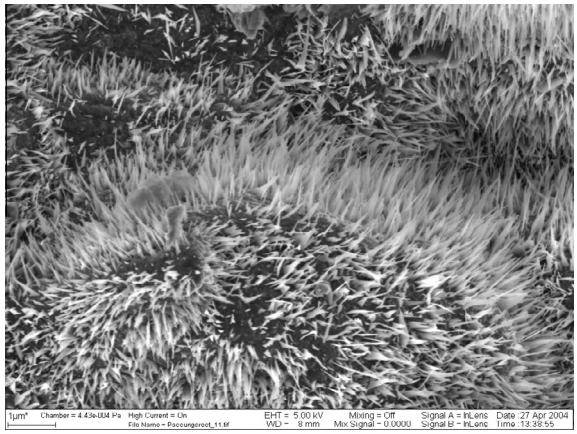

Fig. 28. Enlargement from Fig. 27. Iron oxide whiskers on the crack surface after annealing.

The crack surfaces achieved using all techniques described above showed important basic features of the original crack surfaces whereas some details were not reproduced exactly. The annealing temperature of 240 °C corresponded to the test runs of the steam generator. It was concluded that the first region of the fatigue cracks was formed before the test runs during rail transportation. After installation at the petrochemical plant the test runs led to further crack propagation and annealing of the prior created fatigue crack surfaces.

6. Assessment of the results from analyses and investigations

In the following, the results from the materials testing will be used to derive the mechanism of the failure mode. Additionally, with the results from the vibration tests as well as the experimental and numerical analyses comprising the in-service loading the assumptions made with regard to the main causes of failure will be deduced.

6.1. Results from on-site investigations

As mentioned above a very essential fact may be related to the packaging of the evaporator modules. Fig. 4 shows a module fixed on a transport cradle. It may be noticed that between the tube layers laths were plugged in diagonally as a spacer to stem vertical vibration. According to the manufacturer these laths, originally used for production, were also used in transport. From this picture it may be seen that the laths were not clamped to the tubes in order to prevent displacement. Thus, the chance for displacement of one or more laths during handling or transport may have been very high.

6.2. Results from materials testing

The structure of the steel showed no abnormalities. Because of the bending process the material was extensively deformed and grooves as well as notches were detected at the inside radii of the tube bends.

The starting points of the cracks always were located at the surface of the inside radii. The cracks were identified as circumferential fatigue cracks whereupon the main part of the crack surface (primary fatigue crack area) showed annealing colours which did not correspond to the semi-elliptical rest lines. A second and smaller area of slower fatigue crack propagation followed up which showed less or no annealing colours (secondary fatigue crack area). Thus, materials testing definitely identified the failure mechanism as fatigue cracking.

6.3. Results from vibration tests and finite element analyses

The evaporator modules are a highly complex and nearly un-damped frequency response system. Due to the very low damping even smallest mechanical excitation resulted in high response amplitudes for a certain tube. The analytical estimation of the maximum amplitude corresponded well with that from the finite element analysis. The comparison tests showed that the cracks could be generated without the existence of defects referring to the material or the manufacturing process.

As damage had occurred in longer tubes an excitation by random vibration in the range of the eigenfrequencies of the tubes (9–20 Hz) is most likely to have caused the failure, in contrary to excitation by a single frequency. The frequency range of 9–20 Hz corresponds very well to that the modules were exposed to during the rail transport. The decrease of the eigenfrequency and increase in damping with crack propagation may explain the uniform crack propagation and the equally shaped fatigue crack surfaces.

The fact that only about 2% of the tubes of the evaporator modules showed cracks reinforces the information that at some stage of the handling a few of the laths plugged in between the stacks of tubes for sake of damping were displaced. Experimentally and numerically supported analyses concerning the comparison between the loading stress and the fatigue limit of the bends showed that in case of a missing transportation safeguard the loading stress considerably exceeded the strength of the bends which inevitably may have induced fatigue failure. It is assumed that cyclic stresses did not exceed the fatigue limit when transportation safeguard were present.

7. Root cause of damage

Summarizing the assessment carried out in the above section it may be stated that inappropriate packaging which lead to excessive vibration response throughout the rail transport along 1600 km was the main reason to cause failure on some of the tubes of the evaporator modules. The laths acting as spacers between the tube stacks, as may be seen in Fig. 4, were not secured adequately. Presumably, a few of them got out of place during handling and, hence, some of the tubes could vibrate in vertical direction without sufficient damping during rail transport.

It was estimated that the tube modules may have been exposed to a number of 1.2–1.6 million load cycles during rail transport from the manufacturer's site to the place of installation. It was verified that surface cracks at the inner side of the tube bends may have been easily initiated due to stresses exceeding the fatigue strength of the bends. Hence, the initial cracks were supposed to propagate partly, respectively, totally through the wall thickness, as they did, especially when the test runs were performed. During this phase the surfaces of these fatigue cracks also were annealed when thermally loaded. The second fatigue cracks may have propagated by vibration response during the initial test runs and the crack surfaces may have been annealed afterwards by high temperatures within the steam generator.

8. Conclusions

It has to be mentioned that the process of finding the root cause of failure was a long lasting one. On-site inspections, experimental as well as numerical analyses had to be considered upon, be performed and many discussions had to be fought out. From a long list of hypotheses of potential reasons for failure most items on the list luckily could be rejected step by step with increasing knowledge about the modes and mechanisms behind material, construction and operation.

In consequence, as a corrective step a more effective prevention of transport vibrations was recommended. The transport locks had to be re-designed and realized consequently.

After the failure analysis was completed the damaged modules of the steam generator were repaired without any modification of the basic design. Then, all components were shipped to the site of operation, again, using an upgraded transit lock. After re-installation the unit reached the nominal rating in operation without further failures.

Acknowledgements

The authors wish to thank the customers of the original test report for the permission to publish this failure analysis. The authors wish to thank the following members of BAM staff for their valuable discussions and contributions to the original

test report: Andreas Achelpöhler, Bärbel Bogel, Monika Engelhardt, Matthias Ell, Elke Hoffmann, Thomas Schwertfeger, Kai Singh, Kay v. Oppel, Johann Wimmer.

References

[1] Lange G. Systematic assessment of technical failures (Systematische Beurteilung technischer Schadensfälle), vol. 2. Aufl., Oberursel: Wiley VCH; 1987 [in German].
[2] Becker WT, Shipley RJ. ASM handbook. Failure analysis and prevention, vol. 11. Ohio (USA): ASM Intl.; 2002.
[3] Aurich D, Baer W, Häcker R, Klingbeil D, Ohm K. Analysis and enhancements of fracture mechanical failure concepts; main focus: application of advanced ductile fracture mechanical concepts, ductile-brittle failure transition (Analyse und Weiterentwicklung bruchmechanischer Versagenskonzepte; Schwerpunkt: Anwendung fortgeschrittener zähbruchmechanischer Konzepte; Bruchübergang). BAM-Forschungsbericht 232, Berlin; 1999 [in German].
[4] Aurich D, Eberle A, Guo T, Künecke G, Moussavi Z, Veith H, et al. Analysis and enhancements of fracture mechanical failure concepts; local crack growth, evaluation of the crack resistance from the Charpy impact energy; (Analyse und Weiterentwicklung bruchmechanischer Versagenskonzepte; Lokales Rißwachstum, Ermittlung des Rißwiderstandsverhaltens aus der Kerbschlagarbeit). BAM-Forschungsbericht 192, Berlin; 1993 [in German].
[5] Singh SP, Burgess G. Test protocol for simulating truck and rail vibration and rail impacts in shipments of automotive engine racks. Packag Technol Sci 1995;8:33–41.
[6] Richards D. A report on rail transportation for IEC TC 104 WG15. CEEES Technical Advisory Board for Mechanical Environments. Attachment No. 3, 19th February 2004.
[7] MIL-STD810F. Department of Defense (USA). Test method standard for environmental engineering considerations and laboratory, tests; Method 514.5: Vibration, Figure 514.5C-7 "Rail cargo vibration exposure"; 2000.
[8] ASTM D 4728-01. Standard test method for random vibration testing of shipping containers; 2001.
[9] GAM EG-13. Ministere de la defense (France). Essais generaux en environnement des materiels; 1985.
[10] Kuchling H. Handbook of physics (Taschenbuch der Physik), 15. Auflage, Fachbuchverlag Leipzig, Köln, Leipzig; 1995 [in German].
[11] Beitz W, editor. Dubbel – handbook of mechanical engineering (Dubbel – Taschenbuch für den Maschinenbau), vol. 14. Auflage, Berlin: Springer; 1981 [in German].
[12] ABAQUS user's manual version 6.4. ABAQUS, Inc. 1080 Main Street, Pawtucket, RI, USA; 2003.
[13] Fischer M. Three dimensional numerical simulation of tube bundel vibrations (Dreidimensionale numerische Simulation von Rohrbündelschwingungen). Diss., TU München, 2001-11-21 [in German].
[14] Liu H-H, Cheng W-J, Wang C-J. The mechanism of oxide whisker growth and hot corrosion of hot-dipped Al–Si coated 430 stainless steels in air–NaCl(g) atmosphere. Appl Surf Sci 2011;24:10645–52.
[15] Nakahigashi K, Shimomura Y. Electron microscope observations on nickel oxide whiskers. J Cryst Growth 1975;28:367–71.